

Preparation of AuNPs/MXene nanocomposite for the electrochemical determination of dopamine

Zejun Zhang^{1,2,§}, Yunxiu Sun^{1,§}, Baoli Wang¹, Yijing Ai¹, Fan Shi¹, Yucen Yao¹,
Xueliang Niu³, Wei Sun^{1,*}

¹ Key Laboratory of Laser Technology and Optoelectronic Functional Materials of Hainan Province, Key Laboratory of Functional Materials and Photoelectrochemistry of Haikou, College of Chemistry and Chemical Engineering, Hainan Normal University, Haikou 571158, P. R. China

² College of Chemistry and Chemical Engineering, Zhaotong University, Zhaotong 657000, P. R. China

³ School of Chemistry and Chemical Engineering, Shandong University of Technology, Zibo 255049, P. R. China

[§]These authors contributed equally to this work.

*E-mail: sunwei@hainnu.edu.cn (W. Sun).

Received: 21 February 2022 / Accepted: 15 March 2022 / Published: 5 April 2022

A novel sensing system was constructed by using gold nanoparticles (AuNPs) and MXene-Ti₃C₂T_x nanocomposite decorated glassy carbon electrode (GCE) for dopamine (DA) determination. The AuNPs/MXene nanocomposite was prepared via a drop coating method, which could appreciably enlarge the electrochemically active surface area of as-prepared sensor and promote electron transfer with the enhanced electrochemical signals. Applying AuNPs/MXene/GCE in the optimum conditions, differential pulse voltammetric (DPV) current responses vs. DA concentrations are linear in the wider range of 2.0-500.0 μmol/L along with low detection limit of 0.67 μmol/L (S/N=3). Moreover, the proposed AuNPs/MXene modified GCE exhibited excellent stability, selectivity and reproducibility. Finally, this sensor had been utilized to detect DA successfully in DA hydrochloride injection with satisfactory recoveries, providing a promising application for further sensing analysis.

Keywords: Gold nanoparticles; Ti₃C₂T_x; Dopamine; Electrochemical detection

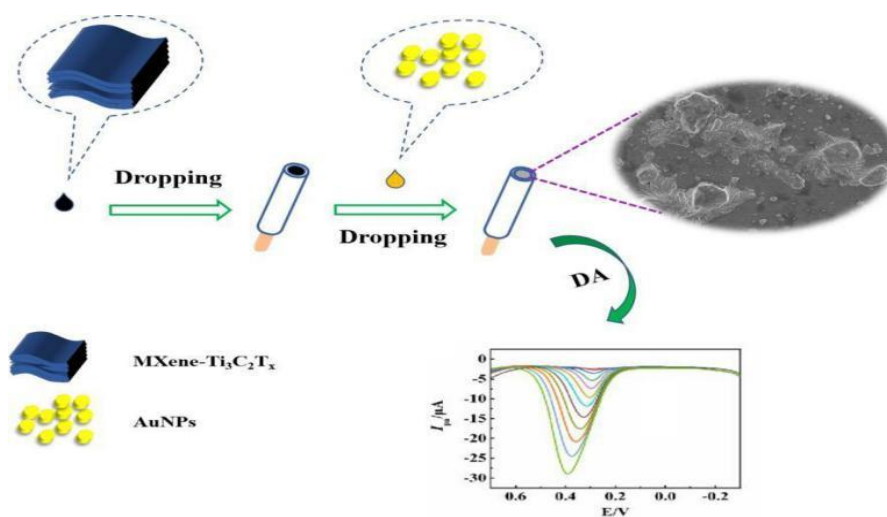
1. INTRODUCTION

Dopamine (DA, 3,4-dihydroxyphenylalanine) is the most abundant catecholamine neurotransmitter in the brain, which has many important physiological functions. The lack of DA in humans may be emerged with the symptoms of neuromuscular disorders, heart failure and others. These symptoms can lead to the serious diseases such as Parkinson's disease, schizophrenia, Alzheimer's

disease, Tourette syndrome and pituitary tumors [1-7]. Therefore, the quantitative and fast determination of DA in various samples is essential. At present, the detection methods of DA mainly include chemiluminescence [8], high-performance liquid chromatography [9,10], colorimetry [11], fluorometry [12-14] and electrochemical sensor [15-19]. Among these methods, electrochemical sensor has many advantages such as simple instruments, convenient operation and high sensitivity, which is widely used in the analysis and detection of DA. Moreover, the electrode modifiers are crucial to increase the performance, so it is of great practical value to explore new kinds of nanocomposites with large specific surface area and good conductivity.

Recently, two-dimensional (2D) materials such as graphene, transition metal carbides and nitrides (MXenes) have been attracting tremendous attentions for their potential applications. MXenes are denoted by the general formula $M_{n+1}X_nT_x$ ($n=1-3$), where M is an early transition metal group, X is carbon and/or nitrogen, and T_x are surface terminal groups (OH, O and/or F). Due to its high specific surface area, abundant surface functional groups and various chemical compositions, MXenes have great potential applications in catalysis [20], energy storage [21], environmental monitoring [22], electrochemical sensors [23-24] and other fields. Among them, titanium carbide ($Ti_3C_2T_x$) is the first reported as well as most studied among the family of MXenes, which has been used in different environmental sensing analysis such as electrochemical detection of bromate, nitrite, phenol and heavy metal ions [25].

Herein, AuNPs and multilayer MXene- $Ti_3C_2T_x$ were immobilized on the surface of glassy carbon electrode (GCE) by drop coating method, which established a new platform for the quantitative and qualitative detection of DA with the process shown in Scheme 1. Electrochemical properties of AuNPs/MXene modified GCE (AuNPs/MXene/GCE) was studied by cyclic voltammetry (CV) and differential pulse voltammetry (DPV) under the optimal conditions. AuNPs/MXene/GCE exhibited a linear response toward DA in a concentration range. Moreover, DA hydrochloride injection sample was analyzed with the recovery from 99.9% to 103.3%. AuNPs/MXene/GCE exhibited excellent stability, selectivity and reproducibility, which provided a promising application for further sensing analysis.



Scheme 1. The preparation process of AuNPs/MXene nanocomposite and determination of DA on AuNPs/MXene/GCE.

2. EXPERIMENTAL

2.1 Reagents

DA (Shanghai Aladdin Bio-Chem Technology Co., Ltd., China), gold nanoparticles (AuNPs) and titanium carbide multilayer nanosheets ($\text{Ti}_3\text{C}_2\text{T}_x$) (Nanjing XFNANO Materials Tech Co., Ltd., China). The ultrapure water was filtered by an IQ7000 instrument (Milli-Q, USA), and all of the reagents were analytically pure and used without further purification.

2.2 Instruments

Transmission electron microscopy (TEM) was carried out using a JEM-2010F microscope (JEOL, Japan) operated at 200 kV with scanning electron microscopy (SEM) performed on a JSM-7600F microscope (JEOL, Japan). UV-Vis spectra were recorded using a UV 5 ultraviolet and visible spectrophotometer (Mettler Toledo, USA). Electrochemical measurements were performed with CHI 660E electrochemical workstation (Shanghai Chenhua Instrument Co., Ltd, China) and a conventional three-electrode system, including the modified GCE ($\Phi=3$ mm) as working electrode, platinum wire electrode and saturated calomel electrode (SCE) as the counter electrode and the reference electrode.

2.3 Preparation of AuNPs/MXene/GCE

GCE was polished by the routine procedure and 6 μL of 2.0 mg/mL $\text{Ti}_3\text{C}_2\text{T}_x$ solution was dropped on the surface of GCE. After drying at room temperature, 8 μL of 0.2 g/L AuNPs were dropped on the MXene/GCE. The modified electrode was denoted as AuNPs/MXene/GCE, which was stored in a refrigerator at about 2 °C when it is not used.

3. RESULTS AND DISCUSSION

3.1 Materials characterizations

The morphologies of MXene- $\text{Ti}_3\text{C}_2\text{T}_x$, AuNPs and AuNPs/MXene nanocomposites were analyzed by SEM. As shown in Fig. 1A, MXene showed a typical accordion-like multilayer structure and smooth surface, and in Fig. 1B AuNPs appeared as particles. As for AuNPs/MXene, AuNPs were densely and randomly exposed to the surrounding or surface of MXene (Fig. 1C). The unique structure of AuNPs/MXene can provide more channels for the adsorption of DA molecules to improve the sensing performance of the modified electrode. TEM image of AuNPs/MXene (Fig. 1D) revealed layered structures with AuNPs, further proving the formation of AuNPs and MXene composite. UV-Vis spectra was performed with AuNPs solution and the mixed solution of AuNPs/MXene. From Fig. 1E, it can be seen that the typical peak position of AuNPs was 530.97 nm and that of AuNPs/MXene was

located at 530.35 nm. The peak position almost did not shift, indicating that the structure of AuNPs remained unchanged after mixing with MXene.

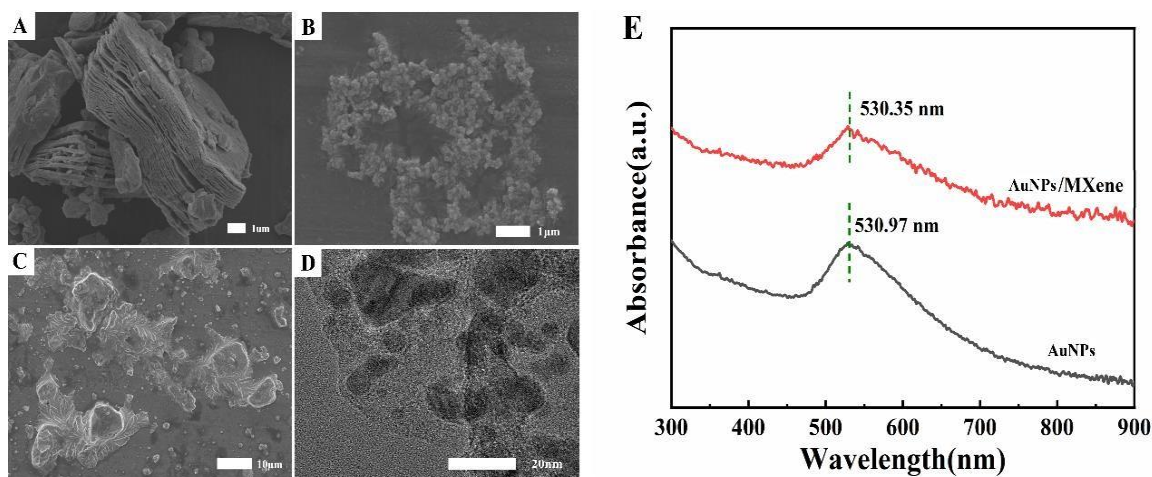


Figure 1. SEM images of (A) MXene, (B) AuNPs and (C) AuNPs/MXene; (D) TEM image of AuNPs/MXene; (E) UV-Vis spectra of AuNPs/MXene and AuNPs.

3.2 Electrode characterizations

Electrochemical impedance spectroscopy (EIS) can reflect the change of resistance on the modified electrode surface with the influence of different materials to electron transfer observed. EIS of each modified electrode were recorded in the mixture of 10.0 mmol/L $K_3[Fe(CN)_6]$ and 0.5 mol/L KCl, and the scan frequency range was 0.01-1 $\times 10^5$ Hz. As shown in Fig. 2A, the charge transfer resistance (R_{ct}) corresponding to electron transfer process was calculated by the diameter of the semicircular at high frequency. The R_{ct} values for bare GCE, MXene/GCE and AuNPs/MXene/GCE were 1147.08 Ω , 1109.47 Ω and 445.41 Ω , respectively. The R_{ct} of AuNPs/MXene/GCE showed the smallest value, indicating that the AuNPs/MXene/GCE promoted electron transfer and improved the conductivity of the electrode surface.

The effective surface area of AuNPs/MXene/GCE was checked at different scan speeds (v) by cyclic voltammetry (CV) with 1.0 mmol/L $K_3[Fe(CN)_6]$ solution. As shown in Fig. 2B, the redox peak current showed a good linear relationship with $v^{1/2}$, obeying the linear regression equations of I_{pc} (μA) = $39.34 \cdot v^{1/2} + 11.40$ ($n=10$, $R^2=0.994$) and I_{pa} (μA) = $-34.68 \cdot v^{1/2} - 13.33$ ($n=10$, $R^2=0.991$). According to the *Randles-Sevcik* equation: $I_p = (2.69 \times 10^5) n^{3/2} A D^{1/2} C_0 v^{1/2}$, where n represents the number of electron transfer, A represents the effective area of the electrode (cm^2), D represents the diffusion coefficient of potassium ferricyanide ($5.7 \times 10^{-6} cm^2/s$), C_0 is the concentration of potassium ferricyanide (1.0 mmol/L), v is the scan speeds (V/s). The effective area of AuNPs/MXene/GCE was calculated as 0.111 cm^2 , while that of GCE was 0.071 cm^2 . Therefore, the GCE modified with AuNPs and MXene provided a larger effective area for the electrochemical reaction.

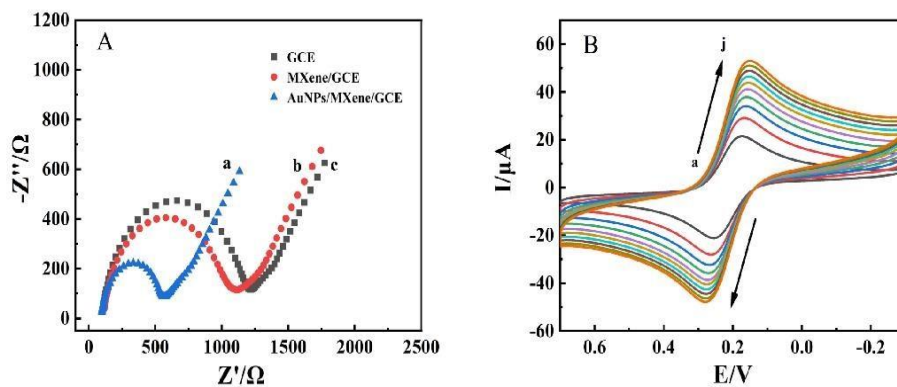


Figure 2. (A) EIS of different modified electrodes in 10.0 mmol/L $K_3[Fe(CN)_6]$ and 0.5 mol/L KCl mixed electrolyte at scan frequencies of $0.01-1 \times 10^5$ Hz, (a) AuNPs/MXene/GCE, (b) MXene/GCE, (c) GCE. (B) Cyclic voltammetric curves of AuNPs/MXene/GCE at different scan speeds in mixed electrolyte (1.0 mmol/L $K_3[Fe(CN)_6]$ and 0.5 mol/L KCl, a→j : 0.1, 0.2, 0.3, 0.4, 0.5, 0.6, 0.7, 0.8, 0.9, 1.0 V/s).

3.3 Electrochemical behaviors of DA

The electrochemical responses of 1.0×10^{-4} mol/L DA solution on different electrodes were studied by cyclic voltammetry. It can be seen from Fig. 3A that the redox peak currents on AuNPs/MXene/GCE are more obvious than those on MXene/GCE and AuNPs/GCE. Table 1 summarized the electrochemical parameters of DA on different modified electrodes. The anodic peak current (I_{pa}) of DA at AuNPs/MXene/GCE was 1.5 and 1.26 times larger than that at MXene/GCE and AuNPs/GCE, respectively. The redox peak currents were increased due to the high conductivity of MXene and AuNPs, and the combination of MXene and AuNPs improves the electron transfer rate and electrochemical responses.

The effects of pH on the direct electrochemical behaviors of DA on AuNPs/MXene/GCE were studied by CV (Fig. 3B). It can be seen that the I_{pa} gradually increased with the increase of pH (2.0-7.0) and reached the maximum at pH 6.0. When the pH value was higher than 6.0, I_{pa} gradually decreased. Therefore, pH 6.0 PBS was selected as the supporting electrolyte. The linear relationship between E^0 and pH was got as $E^0(V) = -0.069 \text{ pH} + 0.664$ ($n=6$, $R^2=0.990$). The slope value was close to the theoretical value of Nernst equation (59 mV/pH), which proved that the number of electron and proton transfer in the redox reaction of DA was equal.

Fig. 3C showed the effect of scan speeds (20-1000 mV/s) for the electrochemical behavior of 1.0×10^{-4} mol/L DA solution on AuNPs/MXene/GCE. The redox peak currents gradually increased with the increase of scan speed with the equations as $I_{pa} (\mu A) = 6.7278 \cdot v (V/s) + 3.0676$ ($n=10$, $R^2=0.9939$) and $I_{pc} (\mu A) = -6.4242 \cdot v (V/s) - 2.5713$ ($n=10$, $R^2=0.9945$). Therefore, the electrochemical oxidation of DA on the modified electrode was a typical adsorptive controlled process. In addition, E_p showed a linear relationship with $\ln v$ and the linear regression equations were $E_{pa} (V) = 0.0268 \ln v + 0.3374$ ($n=6$, $R^2=0.9926$) and $E_{pc} (V) = -0.0188 \ln v + 0.1760$ ($n=6$, $R^2=0.9936$). Based on *Laviron's* equation, the values of electron transfer coefficient (α) and electron transfer number (n) were calculated as 0.59 and 2.32

(close to theoretical value 2), respectively. It can be observed that α value was close to the reported values [26-28]. Therefore, the oxidation of DA on AuNPs/MXene/GCE was a two-protons and two-electrons reaction process. The calculated result of electron transfer rate constant (k_s) was further got as 1.5 s^{-1} . Compared with the references [29-31], the larger k_s value indicated that the modification of AuNPs/MXene made the electronic exchange faster, which provided a favorable conductive electronic sensing platform.

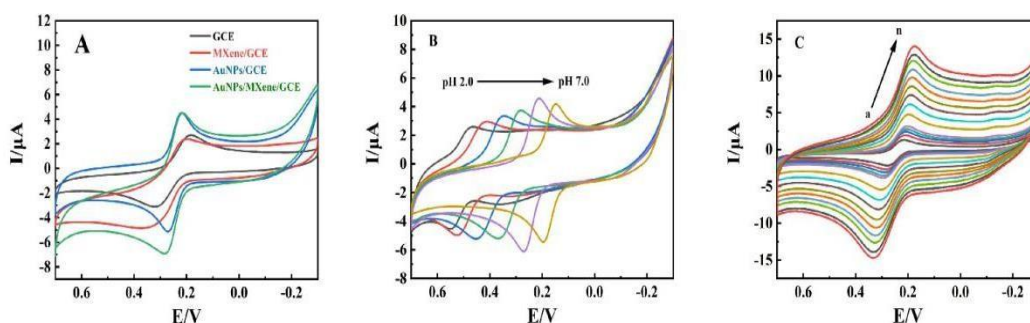


Figure 3. (A) Cyclic voltammograms of different modified electrodes at the scan speed of 0.1 V/s; (B) CV curves of AuNPs/MXene/GCE in different pH PBS (from left to right: 2.0, 3.0, 4.0, 5.0, 6.0, 7.0); (C) CV curves at different scan speeds (a→n: 0.02, 0.04, 0.06, 0.08, 0.1, 0.2, 0.3, 0.4, 0.5, 0.6, 0.7, 0.8, 0.9, 1.0 V/s) in pH 6.0 PBS. DA concentration is $1.0 \times 10^{-4} \text{ mol/L}$.

Table 1. Electrochemical parameters of $1.0 \times 10^{-4} \text{ mol/L}$ DA on different modified electrodes in pH 6.0 PBS

Modified electrode	$I_{pa}/\mu\text{A}$	$I_{pc}/\mu\text{A}$	E_{pa}/V	E_{pc}/V	$\Delta E/\text{mV}$	E^0/V	I_{pa}/I_{pc}
GCE	2.674	2.659	0.322	0.184	138	0.253	1.006
MXene/GCE	3.719	3.219	0.372	0.199	173	0.286	1.155
AuNPs/GCE	4.016	3.843	0.271	0.219	52	0.245	1.045
AuNPs/MXene/GCE	5.161	4.846	0.283	0.215	68	0.249	1.065

3.4 Calibration curve

Under the optimized conditions, DPV analysis of DA was performed on AuNPs/MXene/GCE. Fig. 4A showed that stable anodic curves on AuNPs/MXene/GCE in 0.1 mol/L PBS (pH 6.0) with different concentrations of DA. The anodic peak current increases with the increase of DA concentration (c) with good linear relationship between 2.0-500 $\mu\text{mol/L}$ and the linear regression equation is $I_{pa} (\mu\text{A}) = 0.054 C (\mu\text{mol/L}) - 1.16$ ($n=12$, $R^2=0.988$) with the limit of detection (LOD) as 0.67 $\mu\text{mol/L}$ (3σ). Compared with other reported chemical modified electrodes (Table 2), the detection limit

of AuNPs/MXene/GCE was smaller than the reported values of 1.0 $\mu\text{mol/L}$ [32], 3.9 $\mu\text{mol/L}$ [38] and 2.0 $\mu\text{mol/L}$ [39], and the linear range was wider than the reported values of 2.8-30.3 $\mu\text{mol/L}$ [32], 0.25-20 $\mu\text{mol/L}$ [34], 0.4-10 $\mu\text{mol/L}$ [35], 2.0-200 $\mu\text{mol/L}$ [36], 4.0-50 $\mu\text{mol/L}$ [37], 10-90 $\mu\text{mol/L}$ [38] and 10-150 $\mu\text{mol/L}$ [39].

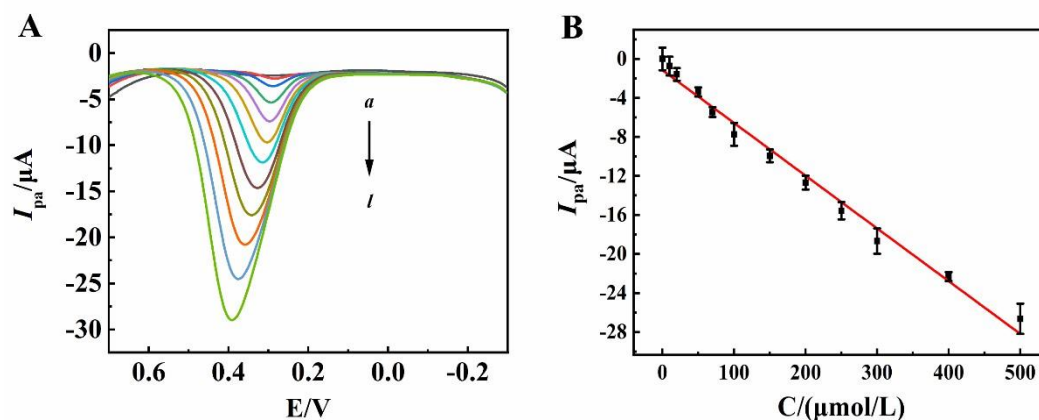


Figure 4. (A) DPV curves of different concentrations of DA at pH 6.0 PBS; (B) The relationship between the anodic peak current and DA concentration (2, 10, 20, 50, 70, 100, 150, 200, 250, 300, 400, 500 $\mu\text{mol/L}$).

Table 2. Comparison of analytical parameters of DA determination with different modified electrodes

Modifiers	Linear range ($\mu\text{mol/L}$)	LOD ($\mu\text{mol/L}$)	References
Tyr-AuNRs-PAMAM/SPCE	2.8-30.3	1.0	[32]
MWCNT/SNFC/Nafion	0.05-100	0.107	[33]
MWCNT@PDOP@PtNPs	0.25-20	0.08	[34]
ESM/Tyr/AgNPs	0.4-10	0.0017	[35]
3D N,P-doped carbon	2.0-200	0.6	[36]
UiO-66-NH ₂ MOF	4.0-50	0.68	[37]
Au-Cu ₂ O/rGO	10-90	3.9	[38]
CeO ₂ /rGO	10-150	2.0	[39]
AuNPs/MXene/GCE	2.0-500	0.67	This work

Tyr, tyrosinase; PAMAM, poly (amido amine); SPCE, screen-printed carbon electrode; MWCNT, multi-walled carbon nanotubes; SNFC, sulfated nanofibrillar cellulose; PDOP, polydopamine; ESM, eggshell membrane; rGO, reduced graphene oxide.

3.5 Actual sample testing

In order to evaluate the practical applications, DA hydrochloride injection was analyzed, which was diluted by pH 6.0 PBS. By using standard addition method, the results were shown in Table 3 with the recoveries of DA in the range of 99.9%-103.3%.

Table 3. Detection of DA hydrochloride injection by AuNPs/MXene/GCE

Sample	Detected ($\mu\text{mol/L}$)	Added ($\mu\text{mol/L}$)	Total ($\mu\text{mol/L}$)	Recovery (%)	RSD (%)
DA hydrochloride injection	45.61	10.00	55.94	103.3	0.64
		20.00	65.59	99.9	3.15
		30.00	75.96	101.2	3.08

3.6 Selectivity, stability and reproducibility

The interference of some common ions and amino acids on the DA analysis was investigated with fixed DA concentration (1.0×10^{-4} mol/L) in PBS (pH 6.0). As shown in Fig. 5A, 1000 times of Ca^{2+} , K^+ , Na^+ , urea, 10 times of glucose, aspartic acid, L-cysteine, and the same concentration of uric acid and ascorbic acid did not interfere with the determination of DA. The stability of AuNPs/MXene/GCE was investigated by cyclic voltammetry (Fig. 5B). The peak current of AuNPs/MXene/GCE remained 99.6% of the initial value after 100 cycles of continuous scanning with RSD of I_{pc} and I_{pa} as 1.17% and 1.95%, indicating the good stability. In addition, the same electrode was measured for 6 times in parallel to evaluate the reproducibility of AuNPs/MXene/GCE. As shown in Fig. 5C, RSD of six parallel measurements was 4.16%. Meanwhile, five identical AuNPs/MXene/GCE were tested for DA, and the RSD value was 4.25%, which proved that AuNPs/MXene/GCE had a good reproducibility.

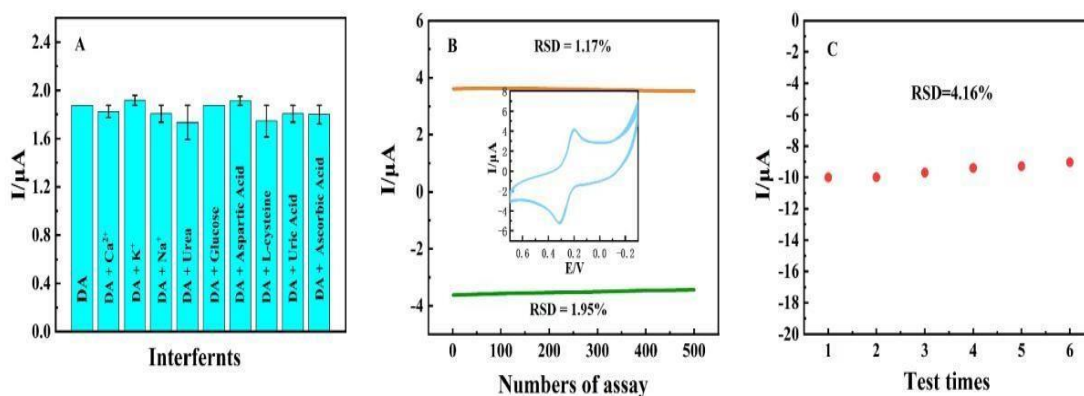


Figure 5. (A) Selectivity; (B) Stability and (C) reproducibility of AuNPs/MXene/GCE in PBS containing 1.0×10^{-4} mol/L DA.

4. CONCLUSION

In this work, AuNPs and MXene were casted on the GCE surface step-by-step, which established a simple and effective sensing platform for the quantification of DA. The modified electrode exhibited excellent sensing performance to DA with the satisfactory linear range (2.0-500 $\mu\text{mol/L}$) and detection limit (0.67 $\mu\text{mol/L}$). DA on the AuNPs/MXene/GCE showed an adsorptive-controlled and two-proton transfer reaction with the electrochemical parameters calculated. The modified electrode showed good selectivity and stability for DA analysis, which was successfully applied for determination of DA in real samples with satisfactory results.

ACKNOWLEDGMENTS

This work is supported by the Shandong Provincial Natural Science Foundation of China (ZR2021MB103), and the National Natural Science Foundation of China (62064004) and the Postgraduate Innovative Research Projects of Hainan Normal University (hsyx2021-5).

References

1. M. Ko, L. Mendecki, A.M. Eagleton, C.G. Durbin, R.M. Stolz, Z. Meng, K.A. Mirica, *J. Am. Chem. Soc.*, 142 (2020) 11717-11733.
2. Y. Li, Y.L. Shen, Y.Y. Zhang, T. Zeng, Q.J. Wan, G.S. Lai, N.J. Yang, *Anal. Chim. Acta*, 1158 (2021) 338419.
3. C.J. Wang, H.X. Shi, M. Yang, Z.R. Yao, B. Zhang, E.Z. Liu, X.Y. Hu, W.M. Xue, J. Fan, *Colloid. Surface. B*, 205 (2021) 111874.
4. K. Promsuwan, A. Soleh, K. Saisahas, J. Saichanapan, P. Kanatharana, P. Thavarungkul, C.X. Guo, C.M. Li, W. Limbut, *J. Colloid Interf. Sci.*, 597 (2021) 314324.
5. V. Sethuraman, T.M. Sridhar, R. Sasikumar, *Mater. Lett.*, 302 (2021) 130387.
6. X.Y. Kang, Y.Y. Song, J.C. Zhao, Y.C. Li, *J. Electroanal. Chem.*, 895 (2021) 115482.
7. S. Lakard, I.A. Pavel, B. Lakard, *Biosensors*, 2021, 11, 179.
8. Y.X. Lan, F. Yuan, T.H. Fereja, C. Wang, B.H. Lou, J.P. Li, G.B. Xu, *Anal. Chem.*, 91 (2019) 2135-2139.
9. X.Y. Hou, W. Huang, Y.K. Tong, M.M. Tian, *Microchim. Acta*, 186 (2019) 68.
10. J. Sun, A.L. Feng, X. Wu, X.W. Che, W.Z. Zhou, *Talanta*, 231 (2021) 122334.
11. S. Rostami, A. Mehdinia, A. Jabbari, E. Kowsari, R. Niroumand, T.J. Booth, *Sensor. Actuator. B Chem.*, 271 (2018) 64-72.
12. S. Abbasi-Moayed, M.R. Hormozi-Nezhad, M. Maaza, *Sensor. Actuator. B Chem.*, 296 (2019) 126691.
13. Z.D. Tang, K. Jiang, S. Sun, S.H. Qian, Y.H. Wang, H.W. Lin, *Analyst*, 144 (2019) 468-473.
14. J. Wang, R. Du, W. Liu, L. Yao, F. Ding, P. Zou, Y.Y. Wang, X.X. Wang, Q.B. Zhao, H.B. Rao, *Sensor. Actuator. B Chem.*, 290 (2019) 125-132.
15. N. Liu, X.P. Xiang, L. Fu, Q. Cao, R. Huang, H. Liu, G. Han, L.D. Wu, *Biosens. Bioelectron.*, 188 (2021) 113340.
16. Y.Y. Sun, Z.R. Song, X. Ni, P. Dramou, H. He, *Microchem. J.*, 169 (2021) 106579.
17. H. Yang, J. Zhao, M.J. Qiu, P. Sun, D.X. Han, L. Niu, G.F. Cui, *Biosens. Bioelectron.*, 124 (2019) 191-198.
18. T. Iranmanesh, M.M. Foroughi, S. Jahani, M.S. Zandi, H.H. Nadiki, *Talanta*, 207 (2020) 120318.

19. N. Diab, D.M. Morales, C. Andronesco, M. Masoud, W. Schuhmann, *Sensor. Actuator. B Chem.*, 285 (2019) 17-23.
20. Y. Chen, X.Q. Xie, X. Xin, Z.R. Tang, Y.J. Xu, *ACS Nano*, 13(2019) 295–304.
21. Q. Li, Q.Z. Wang, L.L. Li, L.J. Yang, Y. Wang, X.H. Wang, H.T. Fang, *Adv. Energy Mater.*, 10(2020) 2000470.
22. M. Naguib, V.N. Mochalin, M.W. Barsoum, Y. Gogotsi, *Adv. Mater.*, 26 (2014) 992–1005.
23. P.A. Rasheed, R.P. Pandey, K. Rasool, K.A. Mahmoud, *Actuator. B Chem.*, 265 (2018) 652-659.
24. D.Y. Wang, D.Z. Zhang, Y. Yang, Q. Mi, J.H. Zhang, L.D. Yu, *ACS Nano*, 15 (2021) 2911-2919.
25. G. Yang, X. Hua, J. Liang, Q. Huang, J.B. Dou, J.W. Tian, F.J. Deng, M.Y. Liu, X.Y. Zhang, Yen Wei, *J. Hazard. Mater.*, 11(2021) 126220.
26. G.L. Luo, Y. Deng, L. Zhu, J. Liu, B.X. Zhang, Y. Zhang, W. Sun, G.J. Li, *Microchim. Acta*, 187(2020)546.
27. J. Cheng, Y.F. Li, J. Zhong, Z.W. Lu, G.T. Wang, M.M. Sun, Y.Y. Jiang, P. Zou, X.X. Wang, Q.B. Zhao, Y.Y. Wang, H.B. Rao, *Chem. Eng. J.*, 3989(2020)125664.
28. H. Cheng, J. Liu, Y.X. Sun, T. Zhou, Q.Y. Yang, S.Y. Zhang, X.P. Zhang, G.J. Li, W. Sun, *RSC Adv.*, 10(2020)42340.
29. Y.X. Sun, B.L. Wang, X.L. He, Y.T. Wang, L. Chen, Y.X. Zhu, G.J. Li, W. Sun, *New J. Chem.*, 45(2021)20396.
30. J. Li, K.Y. Xu, Y. Chen, J. Zhao, P.Y. Du, L.B. Zhang, Z. Zhang, X.Q. Lu, *Chemosensors*, 9(2021)140.
31. S.Y. Liu, F.P. Shi, X.J. Zhao, L. Chen, X.G. Su, *Biosens. Bioelectron.*, 47(2013)379-384.
32. L. Ribovski, F.A. dos Santos, V. Zucolotto, B.C. Janegitz, *J. Solid. State. Electr.*, 23(5) (2019) 1581-1591.
33. V. Durairaj, N. Wester, J. Etula, T. Laurila, J. Lehtonen, O.J. Rojas, N. Pahlmanolis, J. Koskinen, *J. Phys. Chem. C*, 123(40) (2019) 24826-24836.
34. M. Lin, H. Huang, Y. Liu, C. Liang, S. Fei, X. Chen, C. Ni, *Nanotechnology*, 24(6) (2013) 065501.
35. S. Datta, B. Kanjilal, P. Sarkar, *J. Environ. Sci. Health. A Tox. Hazard. Subst. Environ. Eng.*, 53(12) (2018) 1048-1055.
36. L. Zhao, Z. Cai, Q. Yao, T. Zhao, H. Lin, Y. Xiao, X. Chen, *Sensor. Actuat. B: Chem.*, 253 (2017) 1113-1119.
37. N. Wang, M.G. Xie, M.K. Wang, Z.X. Li, X.G. Su, *Talanta*, 220(2020) 121352.
38. T.K. Aparna, R. Sivasubramanian, M.A. Dar, *J. Alloys. Compd.*, 741 (2018) 1130-1141.
39. A. Murali, Y.P. Lan, P.K. Sarswat, M.L. Free, *Mater. Today Chem.*, 12 (2019)222-232.